The impact of temperature volatility on honeybee production

L. Bambagioni[1], G. Buffa[2], E. Fantinato[2], G. V. Lombardi[1], F. Maglione[1], M. E. Mancino[1], G. Toscano[1]

[1] University of Florence, Dept. of Economics and Management

[2]Ca' Foscari University of Venice, Dept. of Environmental Sciences, Informatics and Statistics

28 February 2026

Abstract

We study how climate risk—proxied by the volatility of external temperature—affects honey bee production. We combine sensor data on beehive activity (weight, internal temperature, humidity, and sound pressure) collected by the nature-tech company 3Bee with external weather and air-pollution information from the Copernicus Climate Data Store. Our analysis focuses on Italian beehives over 2020–2024, where sensors transmit at least once every three hours and seasonal production is concentrated between April and October.

Methodologically, we (i) address hive *migration* by building time-varying spatial clusters within altitudinal zones, (ii) filter mechanical beekeeper interventions in weight series, (iii) remove smooth trends and intra-day seasonality nonparametrically, and (iv) estimate weekly integrated variances and covariances using the Fourier-transform estimator of Malliavin and Mancino (2009). Empirically, temperature volatility is positively associated with weight volatility in fixed-effects panels, but explains a limited share of total weight-volatility variation. When measuring weekly productivity by percentage weight change, pooled quantile regressions reveal strong heterogeneity: weight volatility is detrimental in the left tail (hives consuming stores) and beneficial above the median (hives producing), while temperature volatility flips sign from positive at low quantiles to negative in the upper tail. Fine-particulate pollution (PM10) is consistently detrimental across the distribution.

Keywords: climate risk; temperature volatility; honey bee production; high-frequency sensors; Fourier volatility; quantile panel regression.

This work is developed within the PRIN 2022 PNRR project *"Honey BEE VOLatility: An environmental index for assessing climatic risk impact on ecosystem service provision"* (prot. P2022AX5TH; CUP H53D23009460001), funded by the European Union-NextGenerationEU.

1 Introduction

A large body of empirical work on climate impacts has traditionally concentrated on the consequences of changes in average temperature for economic and social outcomes. Early evidence in this direction is provided by Burke et al. (2015), and the approach has since been extended in large-scale international panel settings, such as Kalkuhl and Wenz (2020) and Kahn et al. (2021). In parallel, a newer strand of research argues that focusing on mean shifts alone is incomplete: climate risk also operates through temperature variability, namely short-run "surprises" around long-run trends, which can generate economically and biologically relevant uncertainty even when averages move slowly (Donadelli et al., 2022; Ombadi and Risser, 2022; Kiehl and Winter, 2023; Wu et al., 2024).

In this paper we adopt this latter perspective and bring it to a setting where high-frequency measurement is feasible. Rather than working with low-frequency aggregates, we study the relationship between temperature volatility and honey bee production volatility at high frequency. We exploit beehive-scale sensors that transmit at least every three hours and cover thousands of hives over multiple years. This granular environment allows us to quantify how short-run climate uncertainty translates into variability in biological production, and to assess whether the strength and even the sign of this linkage differ across the distribution of outcomes.

Our empirical investigation is organized around two questions. First, we ask whether higher temperature volatility is associated with higher beehive weight volatility, interpreting the latter as a direct proxy for instability in hive activity and production dynamics. Second, we ask how overall productivity—measured as weekly percentage changes in hive weight—is shaped by volatility in weight and temperature, as well as by other environmental factors. To address the first question, we estimate weekly log-volatilities and run fixed-effects panel regressions linking weight volatility to temperature volatility, controlling for systematic seasonal and spatial heterogeneity. To address the second, we move beyond mean effects and rely on quantile regressions, modeling productivity across

the distribution as a function of volatility measures and pollution, thereby allowing determinants to differ between adverse and favorable production regimes.

Bees are a natural laboratory for this type of analysis. Across ecology, toxicology, and climate science, they are increasingly viewed as sentinels of environmental quality. Their foraging behavior spans wide areas, and through contact with air, water, nectar, and pollen they can accumulate trace contaminants. At the same time, their activity is tightly coupled with climatic conditions that govern flight, foraging efficiency, and plant phenology (Memmott et al., 2007; Le Conte and Navajas, 2008; Kerr et al., 2015). By combining continuous biological sensing with high-frequency climate proxies, we provide a measurement-driven perspective on climate risk that complements traditional ecological field studies and is well suited to capturing short-run uncertainty.

The paper makes four main contributions. First, we develop a high-frequency, nonparametric volatility pipeline for beehive production and climate variables, designed for irregular, sensor-based monitoring. Second, we tackle the data complications created by hive migration, which induces time-varying spatial attribution, and we propose a clustering strategy based on altitudinal zones to match hives with representative external temperature series. Third, we quantify the temperature-volatility channel into production volatility using fixed-effects panel methods. Fourth, we document pronounced distributional heterogeneity in the productivity–volatility relationship via quantile regressions, highlighting that volatility can be beneficial or detrimental depending on whether the hive is in a productive phase or in a consumption/stress phase.

2 Related literature

The closest strands of literature are (i) climate-economy research emphasizing mean temperature effects (Burke et al., 2015; Kalkuhl and Wenz, 2020; Kahn et al., 2021), (ii) emerging work on temperature variability and economic activity (Donadelli et al., 2022; Ombadi and Risser, 2022; Kiehl and Winter, 2023; Wu et al., 2024), and (iii) ecological/biological studies linking environmental factors to bee health and activity (Memmott et al., 2007; Le Conte and Navajas, 2008; Kerr et al., 2015).

Within apiculture, Arias-Calluari et al. (2023) model daily weight variations using a highly parametrized structure on a small sample (10 hives, one day) without a climate connection. O'Connell et al. (2024) study how increased temperatures in glasshouses affect bee activity and brood conditions. Our approach differs by (a) focusing on thousands of hives across years, (b) estimating volatility nonparametrically at high frequency, and (c) integrating external climate and pollution variables.

Methodologically, our volatility estimation builds on the Fourier-transform estimator of Malliavin and Mancino (2009), which is widely used in financial econometrics to estimate integrated (co)variances from discretely sampled data. In our context, it provides an estimator robust to irregular sampling and suited for weekly windows with three-hour measurements.

3 Data

3.1 Beehive sensors (3Bee)

Beehive data are provided by 3Bee, a nature-tech company founded in 2017, which deploys sensor devices to monitor hive activity. For each beehive, the platform collects (at least) weight (kg), internal temperature (°C), humidity (%), and sound pressure (μPa). Transmission times are irregular (asynchronous), but each sensor sends at least once every three hours during active periods.

3.2 External temperature and pollution (Copernicus)

External temperature at 2 meters from ground level is obtained from the Copernicus Climate Data Store. We also use PM10 (particulate matter with diameter ≤ 10 micrometers), available at fine spatial resolution and high frequency. PM10 is a natural proxy for pollution and can affect bees' foraging efficiency by interfering with floral scent cues.

3.3 Migration and time-varying clustering

A distinctive feature of the dataset is *migration*: a non-negligible fraction of hives relocate across locations within a year. This induces *time-varying clustering*, because the same hive may belong to different temperature cells and environmental regimes over time.

Table 1 summarizes the scale of migration by year. The share of migratory hives ranges between 40% and 50%.

Table 1: Migration in the Italian sample

	2020	2021	2022	2023	2024
Total number of hives	810	1756	2675	3460	2818
of which migratory	326	863	1327	1616	1281
(%)	40%	49%	50%	47%	45%

Figure 1 illustrates typical migratory movements within a year.

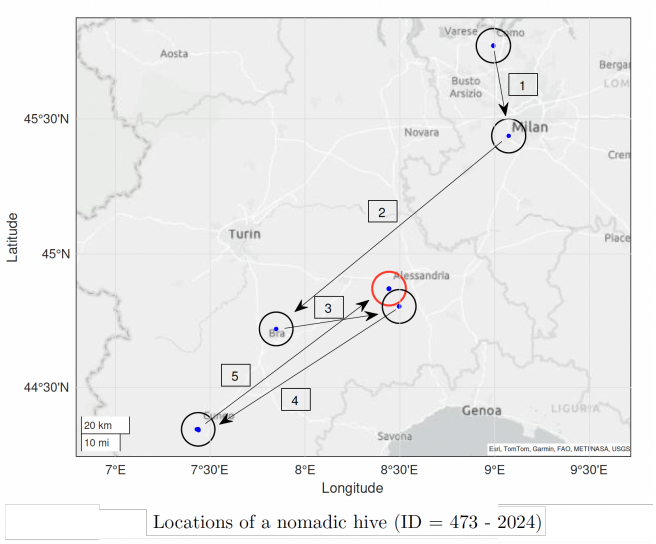

Figure 1: Locations of a migratory hive (illustrative). Migration induces time-varying environmental exposure.

To match external temperature to each hive, we construct spatial clusters within altitudinal zones following the Italian National Institute of Statistics (ISTAT) classification: plains ($h \leq 300$m), hills ($300 < h \leq 600$m), and mountains ($h \geq 600$m), further subdivided into M1 (600–900m), M2 (900–1200m), M3 (≥ 1200m). Within each zone we apply hierarchical clustering with a radius of 7km, consistent with Ziegler et al. (2022) and the typical foraging range.

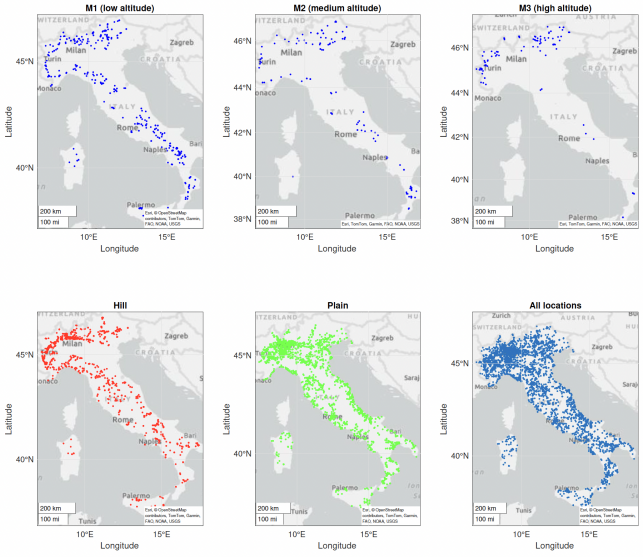

Figure 2: Altitudinal zones and representative clustering (illustrative maps).

3.4 Dataset composition

Tables 2–5 describe the panel composition used in the empirical analysis (non-migratory hives with no missing observations during April–October).

Table 2: Number of observations and cluster size (April–October, pooled)

Year	Abs. freq.	Rel. freq.	N. clusters	Avg. cluster size
2021	4,092	10%	55	74.40
2022	9,114	22%	107	85.18
2023	14,105	34%	141	100.04
2024	14,539	35%	116	125.34
Total	41,850	100%		

Table 3: Number of observations by month (April–October, pooled)

Month	Abs. freq.	Rel. freq.
Apr	5,400	13%
May	5,400	13%
Jun	6,750	16%
Jul	5,400	13%
Aug	6,750	16%
Sep	5,400	13%
Oct	6,750	16%
Total	41,850	100%

Table 4: Number of observations by climate zone (pooled)

Climate zone	Abs. freq.	Rel. freq.
Alpine	5,969	14%
Continental	20,259	48%
Mediterranean	15,622	37%
Total	41,850	100%

Table 5: Number of observations by altitudinal plan (pooled)

Altitudinal plan	Abs. freq.	Rel. freq.
Plane	25,854	62%
Hill	10,571	25%
Mountain	5,425	13%
Total	41,850	100%

4 Preprocessing

4.1 Filtering beekeeper interventions in weight

Weight measurements exhibit occasional abrupt discontinuities due to beekeeper operations (e.g., adding or removing frames, maintenance), which are not part of biological production. We filter such mechanical activity using a jump-removal procedure before volatility estimation. Figure 3 shows an illustrative weight series and its jump-removed version.

Figure 3: Filtering beekeeper activity in weight. The jump-removed series isolates biological dynamics.

4.2 Intraday seasonality and trend removal

Both temperature and hive weight exhibit strong deterministic components: (i) smooth long-run trends and (ii) periodic intraday patterns. Figure 4 illustrates high-frequency temperature dynamics over one week, highlighting a pronounced diurnal cycle.

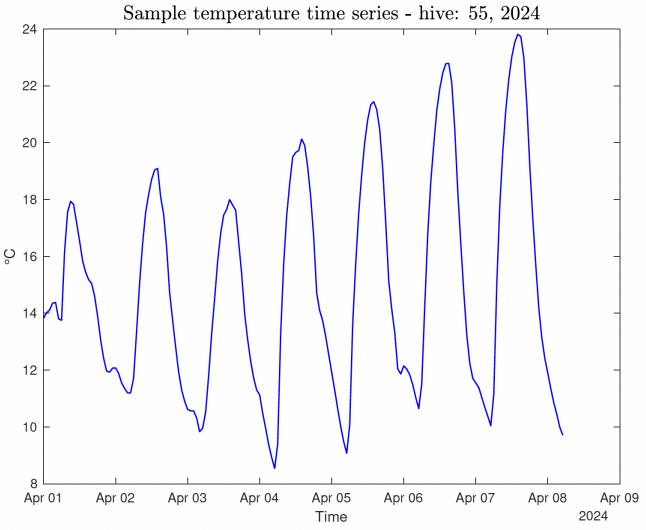

Figure 4: High-frequency external temperature (3-hour grid) over one week: diurnal seasonality.

We remove trend and seasonality non-parametrically following Vogt and Linton (2014), which provides an estimator of a periodic sequence in the presence of a smooth trend. The filtered residuals are then used for integrated (co)variance estimation.

5 Model and estimation

5.1 Data generating process

Fix a weekly interval $[0, T]$ with $T = 1/52$ years and consider a bivariate series $\{(w_j, \tau_j)\}_{j=0}^{n}$ sampled at $t_j = jT/n$, where $n = 56$ corresponds to 3-hour sampling. For $u \in \{w, \tau\}$ we assume (as in Vogt and Linton 2014) that

$$u_j = g_u(t_j/T) + m_{u,j} + \varepsilon_{u,j}, \tag{1}$$

where $g_u(\cdot)$ is smooth, $\{m_{u,j}\}$ is periodic with period θ_u, and $\{\varepsilon_{u,j}\}$ is zero-mean heteroskedastic noise.

We further assume that $\varepsilon_{u,0} \in \mathbb{R}$ and, for $j > 0$,

$$\varepsilon_{u,j} = \eta_{u,j} - \eta_{u,j-1}, \qquad \eta_{u,j} = \eta_u(t_j), \tag{2}$$

with

$$\eta_u(t) = \int_0^t \sigma_u(s)\, dW_u(s), \tag{3}$$

where (W_w, W_τ) is a two-dimensional Brownian motion with instantaneous correlation $\rho(t)$, and $\sigma_u(t)$ is almost surely strictly positive with continuous paths. Under (1)–(3), no parametric functional form is imposed for g_u, $m_{u,j}$, σ_u, or ρ, motivating a nonparametric approach.

5.2 Targets

Our goal is to estimate weekly integrated variances

$$IV_{u,T} = \int_0^T \sigma_u^2(s)\, ds, \qquad u \in \{w, \tau\}, \tag{4}$$

and the integrated covariance

$$IC_{w,\tau,T} = \int_0^T \rho(s)\sigma_w(s)\sigma_\tau(s)\, ds. \tag{5}$$

5.3 Two-step estimation

Step 1 (trend and seasonality). Estimate the sequences $\{g_u(t_j)\}$ and $\{m_{u,j}\}$ using Vogt and Linton (2014) and form filtered residuals

$$\widehat{\varepsilon}_{u,j} = u_j - \widehat{g}_u(t_j) - \widehat{m}_{u,j}. \tag{6}$$

Step 2 (Fourier integrated volatility). Apply the Fourier-transform method of Malliavin and Mancino (2009) to $\{\widehat{\varepsilon}_{u,j}\}$. Let

$$c_k(\widehat{\varepsilon}_u) = \frac{1}{T} \sum_{j=1}^{n} e^{-ik\frac{2\pi}{T}t_j}\, \widehat{\varepsilon}_{u,j}, \tag{7}$$

for integer k, and choose a frequency cut-off N. Define

$$\widehat{IV}_{u,T} = \frac{T^2}{2N+1} \sum_{|k|\le N} c_k(\widehat{\varepsilon}_u)\, c_{-k}(\widehat{\varepsilon}_u), \qquad u \in \{w, \tau\}, \tag{8}$$

and

$$\widehat{IC}_{w,\tau,T} = \frac{T^2}{2N+1} \sum_{|k|\le N} c_k(\widehat{\varepsilon}_w)\, c_{-k}(\widehat{\varepsilon}_\tau). \tag{9}$$

Figure 5 shows an illustrative weekly volatility estimate obtained from filtered residuals.

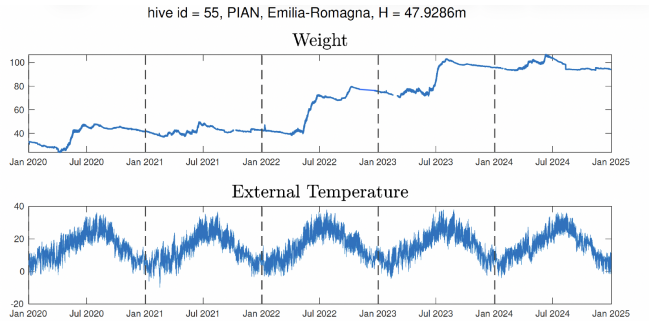

Figure 5: Illustrative weekly integrated variance estimation from filtered residuals.

6 Descriptive statistics

We summarize weekly log-volatilities of temperature and weight, computed from (8) over April–October.

Table 6: Log-volatility of temperature ($\ln \sigma^T$)

	Median	Mean	St.Dev	Skewness	Kurtosis	N. obs
2020	5.03	5.02	0.70	-0.19	2.75	992
2021	4.95	4.93	0.67	-0.33	3.13	4,092
2022	4.91	4.96	0.78	0.03	2.81	9,114
2023	4.91	4.89	0.74	-0.20	2.70	14,105
2024	5.03	4.98	0.83	0.00	2.93	14,539

Temperature log-volatility exhibits relatively small dispersion (vol-of-vol) compared to its mean and is approximately symmetric.

Table 7: Log-volatility of weight ($\ln \sigma^W$)

	Median	Mean	St.Dev	Skewness	Kurtosis	N. obs
2020	1.89	1.86	1.83	0.06	2.77	992
2021	1.71	1.63	1.80	-0.10	3.24	4,092
2022	1.67	1.66	1.91	-0.10	3.03	9,114
2023	1.63	1.50	1.90	-0.79	5.31	14,105
2024	1.58	1.40	2.00	-0.74	4.60	14,539

Weight log-volatility is more dispersed and exhibits fatter tails than temperature log-volatility, consistent with additional biological and management-driven variability.

6.1 Weekly productivity

For each hive and year, define weekly productivity as

$$\Delta^W_{i,t} = \frac{\text{Weight}_{\text{end-week}} - \text{Weight}_{\text{start-week}}}{\text{Weight}_{\text{start-week}}}. \tag{10}$$

Table 8: Weekly weight change (Δ^W)

	Median	Mean	St.Dev	Skewness	Kurtosis	N. obs
2020	-0.0013	0.030	0.103	3.35	18.01	992
2021	-0.0020	0.016	0.076	2.46	12.43	4,092
2022	0.0000	0.026	0.097	3.90	24.41	9,114
2023	-0.0002	0.018	0.081	2.83	16.45	14,105
2024	-0.0006	0.015	0.070	2.34	12.80	14,539

The distribution of Δ^W is positively skewed with fat tails, motivating quantile-based analyses.

7 Empirical analysis

7.1 (A) Linking weight and temperature volatilities

We estimate weekly integrated variances for weight and external temperature and run fixed-effects panel regressions (by year):

$$\ln \sigma^W_{i,t} = \alpha + \text{FE}_t + \text{FE}_{\text{climate}} + \text{FE}_{\text{altitude}} + \beta \ln \sigma^T_{i,t} + \epsilon_{i,t}, \tag{11}$$

where i indexes non-migratory hives with no missing observations and t indexes weeks in April–October. External temperature is observed at the cluster level; we compute robust standard errors clustered at that level.

Table 9: Fixed-effects regressions: $\ln \sigma^W$ on $\ln \sigma^T$

	β			R^2 (within)	R^2 (between)	R^2 (overall)
2020	0.1378	**	(2.54)	0.4222	0.1017	0.3798
2021	0.2022	****	(4.62)	0.2074	0.0637	0.1794
2022	0.1970	****	(5.17)	0.2987	0.0166	0.2407
2023	0.2040	****	(10.39)	0.2411	0.0559	0.1801
2024	0.2223	****	(10.39)	0.1863	0.0548	0.1351

Across years, $\ln \sigma^T$ is positively associated with $\ln \sigma^W$, but (together with fixed effects) explains only about 15–20% of total variation in $\ln \sigma^W$. This suggests that temperature volatility is a meaningful, yet partial, driver of production volatility.

7.2 (B) Explaining productivity: quantile regressions

To study heterogeneous effects across the distribution of productivity, we estimate (pooled, by year) quantile regressions:

$$\Delta^W_{i,t} = \alpha + \text{controls} + \beta^W \ln \sigma^W_{i,t} + \beta^T \ln \sigma^T_{i,t} + \beta^P_1 PM10_{i,t} + \beta^P_2 PM10^2_{i,t} + \epsilon_{i,t}, \tag{12}$$

where controls include month, climate-zone, and altitudinal-plan dummies. Robust standard errors are computed at the cluster level via block bootstrapping (1,000 replications).

We include $PM10^2$ to allow nonlinearities. The marginal effect is

$$\frac{\partial \Delta^W}{\partial PM10} = \beta^P_1 + \beta^P_2 PM10,$$

so a concave negative relationship corresponds to $\beta^P_2 < 0$.

Figure 6 shows an illustrative PM10 data layer.

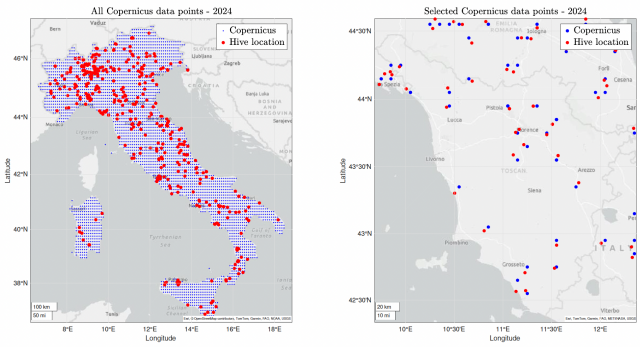

Figure 6: Pollution (PM10): Copernicus high-resolution coverage (illustrative).

7.2.1 Quantile results: 2021–2022

Table 10: Quantile regressions (2021–2022)

		$\ln \sigma^W$		$\ln \sigma^T$		$PM10$		$PM10^2$		pseudo R^2
2021	$q_{0.1}$	-0.0053 (-5.60)	****	0.0064 (3.39)	***	0.0013 (2.79)	***	-0.00002 (-2.06)	**	0.0635
	$q_{0.25}$	-0.0005 (-0.88)		0.0043 (4.29)	****	0.0013 (3.42)	****	-0.00002 (-2.59)	**	0.0275
	$q_{0.5}$	0.0050 (7.10)	****	0.0025 (1.82)	*	0.0019 (5.22)	****	-0.00003 (-3.63)	****	0.0493
	$q_{0.75}$	0.0136 (12.70)	****	0.0010 (0.55)		0.0024 (4.99)	****	-0.00003 (-3.50)	****	0.1644
	$q_{0.9}$	0.0195 (11.81)	****	-0.0051 (-1.81)	*	0.0031 (3.72)	****	-0.00004 (-2.75)	***	0.2418
2022	$q_{0.1}$	-0.0031 (-6.39)	****	0.0014 (1.08)		0.0006 (1.43)		-0.00001 (-1.10)		0.0276
	$q_{0.25}$	0.0009 (2.79)	***	0.0012 (1.21)		0.0004 (1.32)		-0.0000001 (-0.01)		0.0236
	$q_{0.5}$	0.0065 (15.28)	****	-0.0010 (-1.37)		0.0010 (3.86)	****	-0.00001 (-1.78)	*	0.0904
	$q_{0.75}$	0.0125 (16.38)	****	-0.0034 (-2.87)	***	0.0018 (4.03)	****	-0.00002 (-1.79)	*	0.2121
	$q_{0.9}$	0.0167 (11.42)	****	-0.0048 (-2.93)	***	0.0020 (2.60)	***	-0.00001 (-0.63)		0.2974

7.2.2 Quantile results: 2023–2024

Table 11: Quantile regressions (2023–2024)

		$\ln \sigma^W$		$\ln \sigma^T$		$PM10$		$PM10^2$		pseudo R^2
2023	$q_{0.1}$	-0.0034 (-4.30)	****	0.0050 (4.30)	****	0.0001 (0.30)		-0.000003 (-0.47)		0.0395
	$q_{0.25}$	0.0003 (0.93)		0.0025 (3.81)	****	0.0004 (2.09)	**	-0.00001 (-2.06)	**	0.0145
	$q_{0.5}$	0.0052 (7.69)	****	0.0007 (1.26)		0.0010 (4.14)	****	-0.00002 (-3.25)	***	0.0398
	$q_{0.75}$	0.0104 (9.23)	****	-0.0016 (-2.06)	**	0.0016 (4.29)	****	-0.00003 (-3.33)	***	0.1247
	$q_{0.9}$	0.0143 (7.13)	****	-0.0028 (-1.79)	*	0.0018 (2.99)	***	-0.00002 (-2.46)	**	0.1685
2024	$q_{0.1}$	-0.0040 (-11.32)	****	0.0039 (5.09)	****	0.0020 (3.44)	***	-0.0001 (-3.55)	****	0.0476
	$q_{0.25}$	-0.0006 (-1.63)		0.0035 (7.64)	****	0.0016 (4.24)	****	-0.00004 (-3.88)	****	0.0162
	$q_{0.5}$	0.0039 (6.00)	****	0.0021 (3.26)	***	0.0013 (4.47)	****	-0.00003 (-3.84)	****	0.0323
	$q_{0.75}$	0.0091 (9.30)	****	0.0012 (1.25)		0.0015 (3.74)	****	-0.00004 (-3.18)	***	0.1174
	$q_{0.9}$	0.0134 (10.11)	****	0.0001 (0.06)		0.0022 (2.39)	**	-0.0001 (-2.09)	**	0.1749

7.3 Synthesis and interpretation

Table 12 summarizes the sign patterns across quantiles.

Table 12: Impact of volatility and pollution on honey production (Δ^W): sign summary

	$\ln \sigma^W$	$\ln \sigma^T$	$PM10$
10% quantile	−	+	−
25% quantile	0	+	−
Median	+	0	−
75% quantile	+	−	−
90% quantile	+	−	−

The results support a *stage-dependent* interpretation. When a hive is in the left tail of Δ^W (consuming stores or failing to produce), high weight volatility is associated with worse outcomes, while temperature volatility is positively associated. Above the median (productive phase), higher weight volatility correlates with higher production, while higher temperature volatility becomes detrimental at upper quantiles. PM10 is consistently harmful and exhibits evidence of concavity (negative quadratic term) in most years/quantiles.

8 Mechanisms and interpretation

The state-dependent sign patterns in Table 12 are consistent with a simple biological interpretation. When hives are *consuming* (negative or near-zero Δ^W), weight changes are driven by internal consumption and short-lived disturbances. In that regime, a volatile weight path may reflect stress and instability, leading to worse outcomes, while temperature volatility can occasionally be beneficial insofar as it includes short warm spells that facilitate foraging opportunities even in otherwise adverse weeks.

When hives are *producing* (upper quantiles of Δ^W), weight increases reflect net nectar inflows. In that regime, higher weight volatility may be a mechanical consequence of intense foraging cycles and within-week accumulation dynamics, hence its positive association. Temperature volatility, however, becomes negative at high quantiles, consistent with volatility capturing disruptive intraday shocks (e.g., heat spikes or abrupt cooling) that interfere with sustained nectar collection and thermoregulation.

Pollution (PM10) is consistently negative across quantiles, aligning with the idea that particulate matter can degrade floral scent transmission and recognition, lowering foraging efficiency and potentially increasing search costs.

9 Conclusion

We provide evidence that high-frequency temperature volatility is a statistically significant driver of honey bee production volatility, while explaining a limited fraction of its overall variation. Productivity effects are strongly heterogeneous across quantiles: volatility is not uniformly "bad". Weight volatility is detrimental when hives underperform, but beneficial when they are producing; temperature volatility flips sign across the distribution. Pollution (PM10) is consistently adverse. These findings support the view that climate risk should be measured

not only through shifts in mean temperature but also through high-frequency uncertainty, and that ecological production responds in a state-dependent fashion.

Appendix

Regularization of irregular timestamps

Raw sensor transmissions are asynchronous. For each hive-week, we construct a regular three-hour grid and map raw observations to the closest grid point, subject to a maximum tolerance window. If multiple transmissions fall in the same grid cell, we retain the last observation (alternative aggregations yield similar results and can be used as robustness checks). Weeks with insufficient coverage (below a minimum share of filled grid points) are excluded from the baseline panel.

Filtering beekeeper interventions

Let $\Delta w_j = w_j - w_{j-1}$ denote the three-hour increment of the weight series. Mechanical interventions typically appear as isolated, large increments. We implement a threshold-based filter:

$$\Delta w_j^{\text{bio}} = \Delta w_j \, \mathbf{1}\{|\Delta w_j| \le u\}, \qquad w_j^{\text{bio}} = w_0 + \sum_{\ell=1}^{j} \Delta w_\ell^{\text{bio}},$$

with u calibrated from the empirical distribution of increments (e.g., high percentile rules) and cross-validated on hand-labeled intervention episodes when available. Figure 3 illustrates the effect of this filtering step.

Trend and seasonality estimation

We implement the Vogt and Linton (2014) approach to separate a smooth trend $g_u(\cdot)$ from a periodic component $m_{u,j}$. The method can be viewed as combining (i) a local smoothing step for the trend and (ii) a de-trended average over phase-aligned time points for the periodic sequence. In our application, the intraday periodicity is naturally tied to the 24-hour cycle on the 3-hour grid.

Choice of Fourier cut-off

The Fourier estimator (8)–(9) depends on the cut-off N. Conceptually, N trades off bias (too small N discards high-frequency variation) and variance (too large N amplifies noise). Because our weekly windows are short ($n = 56$), we restrict N to a conservative range and verify stability of estimates across plausible values. A pragmatic choice is to scale N with sample size (e.g., $N \propto n^{1/2}$) and check that qualitative regression results are invariant.

Construction of weekly covariates

For each hive-week we compute: (i) $\ln \sigma^W$ from $\widehat{IV}_{w,T}$, (ii) $\ln \sigma^T$ from $\widehat{IV}_{\tau,T}$, (iii) Δ^W from (10), and (iv) weekly PM10 averages on the same spatial cluster as temperature. All regressions include month, climate-zone, and altitude dummies as controls. Standard errors are clustered at the temperature-cluster level.

References

Burke, M., Hsiang, S. M. and Miguel, E. (2015). Global non-linear effect of temperature on economic production. *Nature* **527**, 235–239.

Donadelli, M., Jüppner, M. and Vergalli, S. (2022). Temperature variability and the macroeconomy: A world tour. *Environmental and Resource Economics* **83**, 221–259.

Kahn, M. E., Mohaddes, K., Ng, R. N. C., Pesaran, M. H., Raissi, M. and Yang, J.-C. (2021). Long-term macroeconomic effects of climate change: A cross-country analysis. *Energy Economics* **104**, 105624.

Kalkuhl, M. and Wenz, L. (2020). The impact of climate conditions on economic production: Evidence from a global panel of regions. *Journal of Environmental Economics and Management* **103**, 102360.

Kerr, J. T. et al. (2015). Climate change impacts on bumblebees converge across continents. *Science* **349**(6244), 177–180.

Kiehl, M. and Winter, D. (2023). Estimating the economic impact of temperature volatility. Oxford Economics Research Briefing.

Le Conte, Y. and Navajas, M. (2008). Climate change: impact on honey bee populations and diseases. *Revue Scientifique et Technique (International Office of Epizootics)* **27**(2), 485–497.

Malliavin, P. and Mancino, M. E. (2009). A Fourier transform method for nonparametric estimation of multivariate volatility. *The Annals of Statistics* **37**(4), 1983–2010.

Memmott, J., Craze, P. G., Waser, N. M. and Price, M. V. (2007). Global warming and the disruption of plant–pollinator interactions. *Ecology Letters* **10**(8), 710–717.

Ombadi, M. and Risser, M. D. (2022). What's the temperature tomorrow? Increasing trends in extreme volatility of daily maximum temperature in central and eastern United States (1950–2019). *Weather and Climate Extremes* **38**, 100515.

Arias-Calluari, K., Colin, T., Latty, T., Myerscough, M. and Altmann, E. G. (2023). Modelling daily weight variation in honey bee hives. *PLoS Computational Biology* **19**(3).

O'Connell, D. P., Baker, B. M., Atauri, D. and Jones, J. C. (2024). Increasing temperature and time in glasshouses increases honey bee activity and affects internal brood conditions. *Journal of Insect Physiology* **155**, 104635.

Vogt, M. and Linton, O. (2014). Nonparametric estimation of a periodic sequence in the presence of a smooth trend. *Biometrika* **101**(1), 121–140.

Wu, Q., Shahbaz, M. and Kyriakou, I. (2024). Temperature fluctuations, climate uncertainty, and financing hindrance. *Journal of Regional Science* **65**(1), 112–134.

Ziegler, C., Ueda, R. M., Sinigaglia, T., Kreimeier, F. and Souza, A. M. (2022). Correlation of climatic factors with the weight of an *Apis mellifera* beehive. *Sustainability* **14**(9).